Rapid Communications

Coherent feedback control of two-dimensional excitons

Christopher Rogers,[1,*] Dodd Gray, Jr.,[1] Nathan Bogdanowicz,[1] Takashi Taniguchi,[2] Kenji Watanabe,[2] and Hideo Mabuchi[1,†]
[1]*Ginzton Laboratory, Stanford University, 348 Via Pueblo, Stanford, California 94305, USA*
[2]*National Institute for Materials Science, 1-1 Namiki, Tsukuba 305-0044, Japan*

(Received 19 March 2019; revised manuscript received 15 December 2019; published 31 January 2020)

Electric dipole radiation can be controlled by engineering of the photonic environment. A coherent interaction between forward and backward emission depends interferometrically on the position of a nearby mirror. The transverse coherence of exciton emission in a single layer of $MoSe_2$ and the highly radiatively broadened nature of our samples removes fundamental physical limitations of previous experiments employing pointlike dipoles. This enables full control over the exciton radiative coupling rate and total linewidth at cryogenic temperatures from near zero to 1.8 ± 0.4 meV and from 0.9 to 2.3 ± 0.1 meV, respectively.

DOI: 10.1103/PhysRevResearch.2.012029

The transition metal dichalcogenides (TMDs) $MoSe_2$ and MoS_2 become direct band-gap semiconductors when isolated in monolayer form [1–3], transferring a significant fraction of the interband spectral weight to a strong and spectrally narrow excitonic resonance [4,5]. Coherence [6], spin-valley interactions [7,8], strain effects [9], few-body electron physics [10,11], many-body physics [12–14], and engineered confinement [15,16] have all been studied using TMD excitons. Monolayer and few-layer TMDs were first prepared by mechanical exfoliation [1,2,17] and were typically *n*-doped and inhomogeneously broadened by substrate roughness. Four-wave mixing techniques were used to investigate the interplay among homogeneous, inhomogeneous, and radiative broadening in TMD samples [18–20]. By adding electrostatic control via a gate, the semiconductor could be made neutral [11,12]. Encapsulation of TMDs in atomically flat hBN (hexagonal boron nitride) has enabled further improvements [21–23]. While some residual imperfections persist [24–27], sample qualities sufficient to manifest quantum coherent effects are now achievable.

Electric dipole radiation can be controlled by coherent optical feedback, as has previously been studied by modulating the photonic environment for point dipoles placed both in optical cavities [28–30] and near metal mirrors [31,32]. Modifying the electromagnetic environment by using a mirror to engineer the local photonic density of states can affect the radiative decay rate of a dipole [28,32]. In addition to those involving the electric dipoles of fluorescent molecules [31,32], trapped ions [33,34], and quantum dots [35–37], similar studies have been conducted with surface plasmon-polaritons [38] and with an acoustic gong [39]. For a perfect 0D dipole placed near a perfectly reflective spherical concave mirror, the radiative coupling and total linewidth could in principle be modulated from near zero to twice their vacuum values [32]. Experimentally, this effect is much smaller due to the subunity quantum efficiency of real dipoles and their decoherence properties. The use of planar mirrors (or finite numerical aperture [33]) for practical reasons also partially obscures the interference effect. For a planar mirror, interference effects on the radiative coupling and total linewidth decrease rapidly with mirror-dipole distance because of the high numerical aperture of the emission pattern. However, the situation is different for excitons in two-dimensional systems because the delocalized nature of the planar exciton leads to conservation of transverse momentum [40–42], meaning that the exciton emission is angularly restricted. This opens the possibility of full manipulation of the radiative coupling even when the mirror is many wavelengths from the emitter.

The features that make this system a good test bed for new excitonic and optical physics [43] also make it attractive for engineering applications. Coupling mirror-membrane position to the frequency, linewidth, and strength of a resonance is of interest for optomechanics. Controllably reducing the intrinsic linewidth could greatly enhance the size of this optomechanical coupling relative to linewidth, which is an important metric for these devices. For nonlinear and quantum optics, the relative magnitude of the nonlinear coupling would be similarly advantageous [44,45]. High-quality TMDs grown by chemical vapor deposition [46,47] and then laser annealed to improve sample quality [48] offer a path toward scalable quantum engineering applications by removing the material quality repeatability issues and area restrictions present in exfoliated samples.

We report on the effect of varying the distance between the monolayer semiconductor $MoSe_2$ and a metal mirror on the $MoSe_2$ exciton resonance (X_0). A low-finesse photonic mode is formed between the mirror and $MoSe_2$, and light coupling out of this cavity interferes with light directly emitted by the exciton. As the mirror is translated, the interference condition at the $MoSe_2$ varies between destructive and constructive, strongly modifying the reflection of the device. The

*cmrogers@stanford.edu
†hmabuchi@stanford.edu

Published by the American Physical Society under the terms of the Creative Commons Attribution 4.0 International license. Further distribution of this work must maintain attribution to the author(s) and the published article's title, journal citation, and DOI.

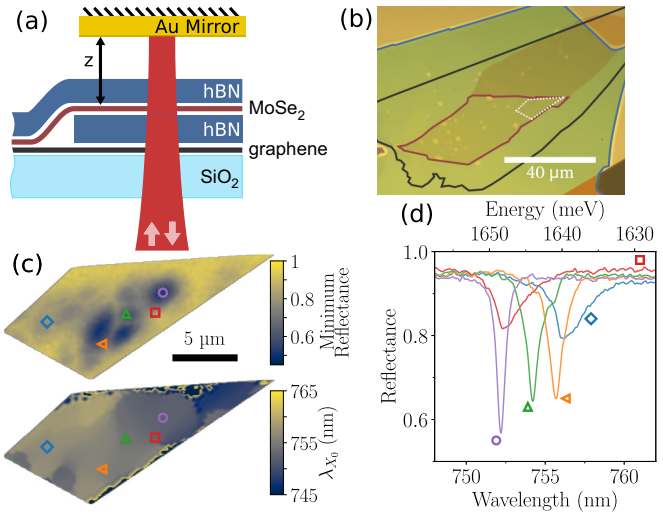

FIG. 1. Sample characterization. (a) A schematic of the heterostructure device. The Au mirror is mounted on a mechanical actuator so that z can be varied. (b) A microscope image of the sample. The monolayer $MoSe_2$ region is outlined in burgundy. A few-layer graphene flake outlined in black on the bottom of the stack electrostatically isolates the $MoSe_2$ from the SiO_2 substrate. The bottom hBN is outlined in blue. (c) Spatial maps of the maximum dip in reflection at X_0, and its center wavelength λ_{X_0} from a region of the sample corresponding to the area outlined with dashed white lines in panel (b). (d) Selected reflection spectra corresponding to the marked positions in panel (c). These spectra were collected at 4 K with the mirror positioned slightly away from maximum destructive interference.

magnitude of the reflection at X_0 can vary from near zero to near unity, and the absorption varies in a complementary way. This interference condition also affects the radiative coupling of X_0 to the environment, and at maximal destructive interference the coupling can be almost entirely suppressed, in theory limited only by mirror losses. Conversely, at maximal constructive interference, this coupling is twice its vacuum value. Since X_0 is primarily radiatively broadened (a ratio of up to 3:1 in our samples, enabled by recent advances in two-dimensional [2D] material sample fabrication [21–23]), this modulation of the radiative coupling from near zero to 1.8 ± 0.4 meV induces a similar effect on the total linewidth from 0.9 to 2.3 ± 0.1 meV.

We fabricate heterostructures of $MoSe_2$ encapsulated in hBN and then transfer these stacks onto fused silica substrates [49,50]. A microscope image of the sample used for the data presented in this paper is shown in Fig. 1(b), and a schematic of the experiment is shown in Fig. 1(a). Experiments are conducted within an optical cryostat at 4 K. A gold mirror on a mechanical actuator is placed in close proximity to the $MoSe_2$ heterostructure. The mirror is translated along the optical axis, and at selected z positions reflectance measurements are made using a grating spectrometer. Measurements were automated using the PYTHON instrument control package Instrumental [51]. Note that z is the *optical* path length between the mirror and the $MoSe_2$. This method of mirror translation isolates the effect of coherent electromagnetic feedback since it is entirely free of coupling to strain or electric field in the TMD. More experimental details can be found in Ref. [52]. Because we excite with ∼15 nW of optical power, the excitation occupation number during the measurement is very low, $\sim 10^{-3}$ [52]. Thus, our experiments correspond to probing radiative reaction in the regime of perturbative quantum electrodynamics [53].

Maps of the magnitude of the dip in reflectance at X_0 and its center frequency and wavelength (ω_{X_0}, λ_{X_0}) are shown in Fig. 1(c). The mirror is near but not at maximum destructive interference. As observed by others [21,22], there is inhomogeneity on a few-micron scale in both λ_{X_0} and the magnitude of the reflection. Nonetheless, some areas of the sample are radiatively broadened. In Fig. 1(d), spots are selected to show both a range of sample quality and λ_{X_0}.

A heat map of the reflectance as a function of mirror position is shown in Fig. 2(a), along with selected line cuts of the same data in Fig. 2(c). The X_0 resonance appears as a dip (the central bright band) that varies in magnitude, width, and center frequency as the mirror is translated across a full fringe. We define z_d and z_c as the mirror positions for maximal destructive and constructive interference respectively, as in Fig. 2(b). When the reflection from the mirror interferes destructively with that from the $MoSe_2$, the radiative coupling of X_0 becomes very small and the dip disappears below the noise floor [$z_{d,1}$ and $z_{d,2}$ in Fig. 2(a)]. Surprisingly, the minimum reflection over z does not occur at z_c, but rather occurs at each of two mirror positions on either side of z_c. At these two reflection minima ($z_{m,1} = 835$ nm and $z_{m,2} = 1015$ nm), the reflectance is ≈6%, while in between it reaches 43% at z_c.

This surprising effect is due to an interplay between the radiative coupling rate (γ_r) and nonradiative coupling rate (γ_{nr}). At z_c, constructive interference leads to maximal radiative broadening. Here, the exciton is primarily radiatively broadened and γ_r is larger than $\gamma_{nr} + \gamma_{ib,\mathrm{eff}}$. We define $\gamma_{\mathrm{tot}} = \gamma_r + \gamma_{nr} + \gamma_{ib,\mathrm{eff}}$ as the total linewidth, where $\gamma_{ib,\mathrm{eff}}$ is the effective contribution to the total linewidth from a constant Gaussian inhomogeneous broadening γ_{ib}. Please see Refs. [52,54,55] for more details of the subtle difference between γ_{ib} and $\gamma_{ib,\mathrm{eff}}$. For most purposes, γ_{ib} and $\gamma_{ib,\mathrm{eff}}$ can be thought of as equivalent.

We note that in an ideal material ($\gamma_r \gg \gamma_{nr}, \gamma_{ib,\mathrm{eff}}$) the reflectance feature at z_c would be very small and the minimum reflectance would approach unity. However, in our real sample, γ_{nr} and $\gamma_{ib,\mathrm{eff}}$ increase the depth of the reflectance feature at z_c so that the minimum reflectance is 43%. This occurs because the intrinsic reflectivity of the exciton is a metric of the ratio $\gamma_r/\gamma_{\mathrm{tot}}$ [22]. As this ratio increases, the intrinsic reflectivity of the exciton becomes higher and the reflectance feature becomes smaller. When the mirror is moved in either direction from z_c, the decrease in γ_r causes the ratio γ_r/γ_{nr} to be reduced. This causes the exciton to absorb more light, and the reflectance feature deepens until reaching its minimum value at $z_{m,1/2}$. At $z_{m,1/2}$, impedance matching leads to a maximum absorption of near unity. The exciton also begins to spectrally narrow, since the contribution of γ_r to the total linewidth is reduced. As the mirror is moved past $z_{m,1/2}$ and toward destructive interference at $z_{d,1/2}$, γ_r continues to decrease. This causes the X_0 feature to shrink and spectrally narrow until it eventually disappears. Near $z_{d,1/2}$, the total linewidth is dominated by γ_{nr} and $\gamma_{ib,\mathrm{eff}}$, so that $\gamma_{\mathrm{tot}} \approx \gamma_{nr} + \gamma_{ib,\mathrm{eff}}$.

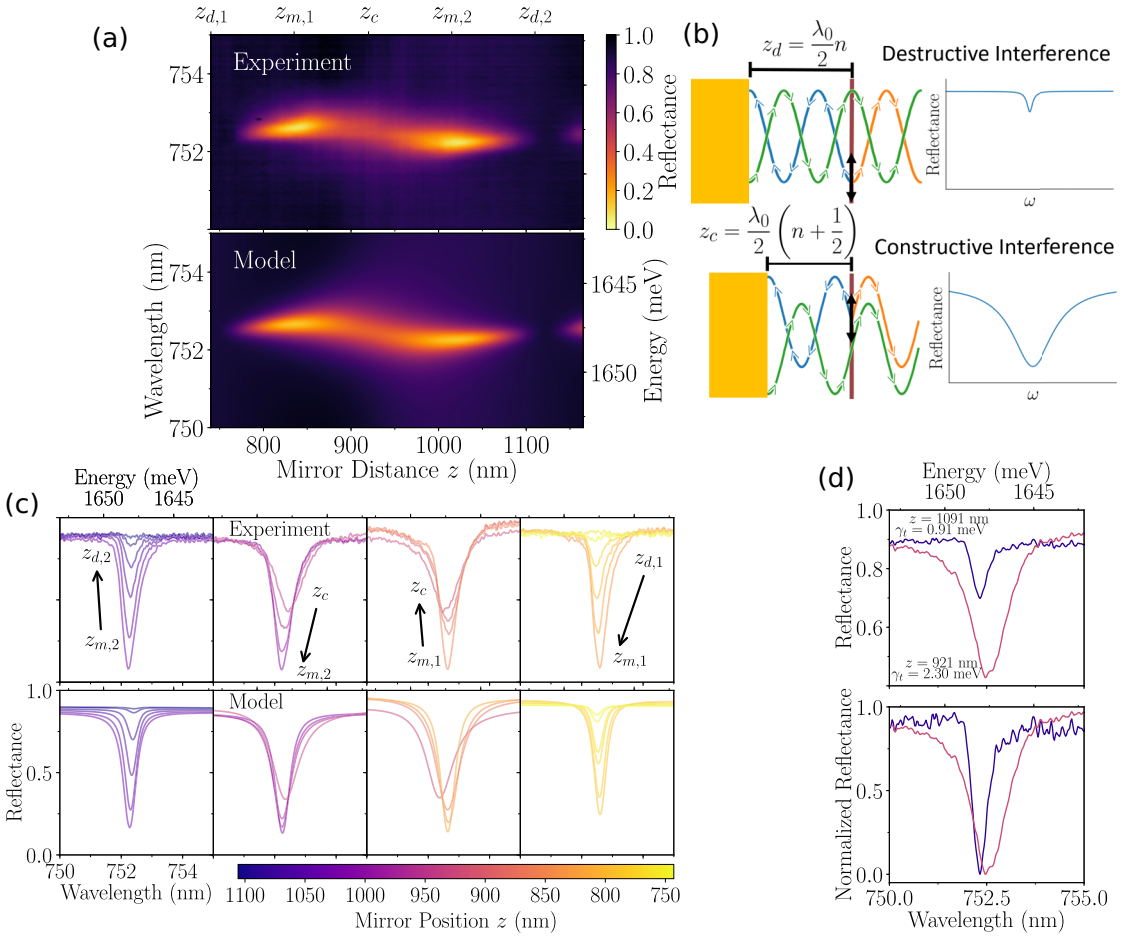

FIG. 2. Experimental and modeled reflectance. (a) Measured and modeled reflectance spectra near the X_0 resonance as z is varied over a full fringe. Measurements at 4 K. Note that these data come from near the region marked with a purple circle in Fig. 1(c). (b) A schematic representation of the effect of mirror position z on the the exciton resonance. The black double-headed arrow represents the exciton electric dipole, and the blue and orange curves represent the electric field emitted toward and away from the mirror, respectively. The electric field reflected by the mirror is represented in green. To the right of the monolayer, the fields interfere either constructively or destructively depending on mirror position. The corresponding schematic plots represent the modulation of amplitude and linewidth of the X_0 feature. The z_d and z_c values, shown for the destructive and constructive interference cases respectively, assume a perfect mirror with zero skin depth. For simplicity, multiple reflections and the full heterostructure have been omitted. (c) Selected line cuts of the measured and modeled reflectance in the spectral region of X_0. The black arrows indicate increasing z. (d) Measured reflectance, both absolute and normalized, at two z positions highlighting the modulation of total linewidth.

Note that the center frequency ω_{X_0} of the dip changes with mirror position as well. When the light reflected from the mirror is exactly in or out of phase with that back-emitted from the $MoSe_2$, the dip is at its vacuum frequency (ω_0), and $\omega_{X_0} = \omega_0$. However, away from either of these positions, dispersion over the X_0 resonance causes a spectrally asymmetric interference condition, which shifts the effective line center ω_{X_0}.

We model the TMD exciton using a Lorentzian susceptibility, which accounts for radiative broadening γ_r and nonradiative broadening γ_{nr} [22,56]:

$$\chi_{\text{exc}} = -\frac{c}{\omega_0 d}\frac{\gamma_{r,0}}{\omega - \omega_0 + \frac{i\gamma_{nr}}{2}}, \tag{1}$$

where ω_0 is the exciton vacuum center frequency, ω is the optical frequency, c is the speed of light, and d is the $MoSe_2$ thickness. The homogeneous reflectance $R_{\omega_0}(\omega)$ is calculated for the full heterostructure and mirror stack using a transfer matrix method [57]. Inhomogeneous broadening effects are included by convolving $R_{\omega_0}(\omega)$ with a Gaussian of characteristic width γ_{ib} to obtain the full reflectance $R(\omega)$. Selected line cuts and their z positions were simultaneously fit to this model to find global values for γ_r, γ_{nr}, γ_{ib}, and ω_{X_0}; see Ref. [52] for more details. Plots of the modeled reflectance are shown in Figs. 2(a) and 2(c). Both qualitatively and quantitatively the model matches closely with the experimental data. See Ref. [52] for a discussion of the small discrepancies, an estimate of the uncertainty in the fitted parameters, and a comparison of two different methods for extracting the z position.

From both the experimental data and the model, we extract full-width-half-maximum (FWHM) linewidths, which are shown in Fig. 3(a). As a function of mirror position, the linewidth γ_{tot} varies from ∼0.9 meV near z_d to ∼2.3 meV at z_c for a total modulation of ∼2.5×, while in the model it varies from 0.9 to 2.4 meV, or ∼2.6×. This modulation

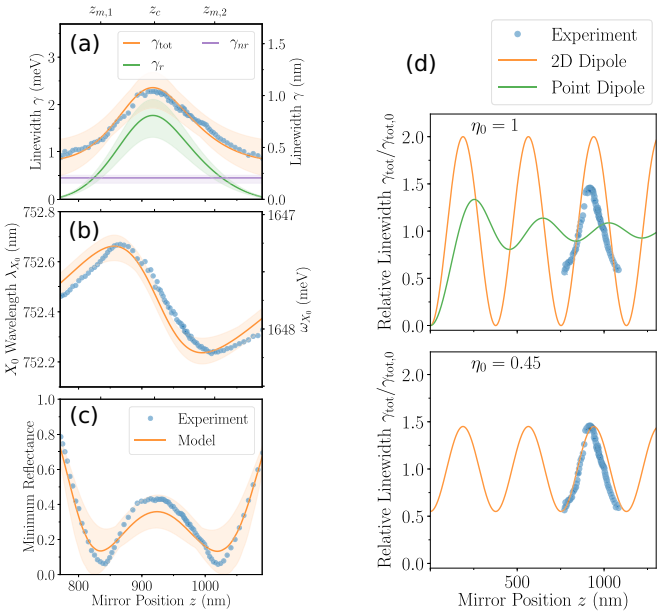

FIG. 3. Extracted and modeled linewidths. (a) The FWHM linewidth $\gamma_{\rm tot}$ both from the model and extracted from the experimental data. Note that we cannot extract linewidth data over the full range of the experimental data, since near z_d the X_0 resonance is almost completely extinguished. Also shown are γ_r and γ_{nr} from the model. (b) Center frequency ω_{X_0} for both model and experiment. (c) Minimum reflectance for both model and experiment. The shading in panels (a)–(c) represents the uncertainties in the model; see Ref. [52]. (d) Simplified models of the total linewidth modulation for both a point and 2D dipole, assuming a perfect mirror with zero skin depth. The top panel shows the ideal case with coherent quantum efficiency in vacuum $\eta_0 = 1$, and the bottom panel shows the case with $\eta_0 = 0.45$. Both are shown alongside the experimental data.

can also be clearly seen in Fig. 2(d). The change in γ_r of the X_0 resonance is the primary cause of the change in $\gamma_{\rm tot}$, and the values of γ_r extracted from the model vary from near zero at z_d to 1.8 ± 0.4 meV (440 ± 100 GHz) at z_c. Near z_d, $\gamma_{\rm tot}$ is dominated by the contribution of γ_{nr} and $\gamma_{ib,\rm eff}$, while at z_c, radiative coupling dominates, with a ratio of $\gamma_r/(\gamma_{nr} + \gamma_{ib,\rm eff}) \sim 3$.

Modeled and experimental values for ω_{X_0} and the minimum reflectance shown in Figs. 3(b) and 3(c) agree as well. The line shift of $\approx$1 meV (240 GHz) is significant relative to $\gamma_{\rm tot}$.

Lastly, in Fig. 3(d) we compare our data to a simplified model of both a 2D dipole and a point dipole. The 2D case highlights that the transverse coherence and delocalized nature of the exciton causes light emission into specific modes rather than the full numerical aperture. We define the coherent quantum efficiency in vacuum $\eta_0 = \gamma_{r,0}/\gamma_{\rm tot}$, which differs from the incoherent quantum efficiency $\gamma_{r,0}/(\gamma_{r,0} + \gamma_{nr})$. For our purpose, η_0 is the relevant quantity because the linewidth modulation effect depends on the coherent interference of emitted waves. For a 2D dipole, the total linewidth $\gamma_{\rm tot}(x)$ as a function of normalized mirror position $x = \frac{4\pi z}{\lambda_0}$ is [52]

$$\frac{\gamma_{\rm tot}(x)}{\gamma_{\rm tot,0}} = 1 - \eta_0 \cos x, \tag{2}$$

where $\gamma_{\rm tot,0}$ is the total linewidth in vacuum and λ_0 is the wavelength in vacuum. The equivalent expression for a 0D dipole is given in Ref. [52].

It is clear that for an ideal 2D dipole ($\eta_0 = 1$) and a perfect planar mirror, the linewidth can be fully modulated even when the mirror is far from the dipole. This is not true in the 0D dipole case, because integrating emission over the full numerical aperture obscures the interference effect as z increases. Also shown is a plot for $\eta_0 = 0.45$ chosen to match the superimposed experimental data.

As can be seen clearly in Fig. 3(d), no 0D dipole in front of a flat mirror (even with a perfect mirror and $\eta_0 = 1$) could produce the behavior seen in the experiments. While defects and inhomogeneity likely prevent the excitons from being delocalized over the entire excitation area, the amplitude and phase of the experimental $\gamma_{\rm tot}$ is strong evidence that they are delocalized on a length scale of the same order as the optical wavelength.

We have demonstrated coherent control over an exciton resonance by positioning a mirror in close proximity to the monolayer semiconductor $MoSe_2$, showing near complete modulation of the reflection at X_0. The concurrent change in radiative coupling rate induces a change in total linewidth of $\sim$2.5×, demonstrating the dominant role of radiative coupling for excitons in monolayer $MoSe_2$ and serving as an important verification of theoretical models used to describe excitonic physics in TMD materials. For engineering applications, the modulation of the X_0 resonance could greatly enhance optomechanical couplings, while the effective enhancement of nonlinearities [44] is useful for nonlinear optics and quantum optics. Our strain-free and DC-electric-field-free method of mirror positioning has allowed us to study the underlying photonic interference effect present in the system, and the unprecedented control over the radiative coupling of an excitonic resonance paves the way for many future experiments.

Note added. During preparation of this paper, we became aware of preprints presenting similar work by Y. Zhou *et al.* [58], H. H. Fang *et al.* [59], and J. Horng *et al.* [60]. See Ref. [52] for a short discussion of where the results presented here fit in the context of these similar works.

This work was funded in part by the National Science Foundation (NSF) Awards No. PHY-1648807 and No. DMR-1838497 and also by a seed grant from the Precourt Institute for Energy at Stanford University. Part of this work was performed at the Stanford Nano Shared Facilities (SNSF), supported by the NSF under Award No. ECCS-1542152. C.R., D.G., and N.B. were supported in part by Stanford Graduate Fellowships. C.R. was also supported in part by a Natural Sciences and Engineering Research Council of Canada doctoral postgraduate scholarship. K.W. and T.T. acknowledge support from the Elemental Strategy Initiative conducted by the MEXT, Japan, and and the CREST (JPMJCR15F3), JST. All authors thank Tatsuhiro Onodera for discussions relating to the reflectance model. All authors thank Daniel B. S. Soh and Eric Chatterjee for discussions relating to exciton physics. C.R. thanks Joe Finney, Giovanni Scuri, and Elyse Barre for help with heterostructure fabrication, Logan Wright for pointing out relevant litera-

ture, and Peter L. McMahon for suggestions relating to the manuscript. C.R. conceived the experiments, fabricated the samples, performed the experiments, and performed the data analysis. C.R. and D.G. built the confocal microscope setup for the cryostat, as well as the grating spectrometer. C.R. and N.B. automated the measurements. T.T. and K.W. grew the hBN. C.R., N.B., D.G., and H.M. all contributed to the manuscript.

[1] K. F. Mak, C. Lee, J. Hone, J. Shan, and T. F. Heinz, Atomically Thin MoS_2: A New Direct-Gap Semiconductor, Phys. Rev. Lett. **105**, 136805 (2010).

[2] A. Splendiani, L. Sun, Y. Zhang, T. Li, J. Kim, C.-Y. Chim, G. Galli, and F. Wang, Emerging photoluminescence in monolayer MoS_2, Nano Lett. **10**, 1271 (2010).

[3] Y. Zhang, T.-R. Chang, B. Zhou, Y.-T. Cui, H. Yan, Z. Liu, F. Schmitt, J. Lee, R. Moore, Y. Chen, H. Lin, H.-T. Jeng, S.-K. Mo, Z. Hussain, A. Bansil, and Z.-X. Shen, Direct observation of the transition from indirect to direct bandgap in atomically thin epitaxial MoSe2, Nat. Nanotechnol. **9**, 111 (2013).

[4] A. Molina-Sánchez, D. Sangalli, K. Hummer, A. Marini, and L. Wirtz, Effect of spin-orbit interaction on the optical spectra of single-layer, double-layer, and bulk MoS_2, Phys. Rev. B **88**, 045412 (2013).

[5] A. Molina-Sánchez, M. Palummo, A. Marini, and L. Wirtz, Temperature-dependent excitonic effects in the optical properties of single-layer MoS_2, Phys. Rev. B **93**, 155435 (2016).

[6] A. M. Jones, H. Yu, N. J. Ghimire, S. Wu, G. Aivazian, J. S. Ross, B. Zhao, J. Yan, D. G. Mandrus, D. Xiao, W. Yao, and X. Xu, Optical generation of excitonic valley coherence in monolayer WSe_2, Nat. Nanotechnol. **8**, 634 (2013).

[7] D. Xiao, G.-B. Liu, W. Feng, X. Xu, and W. Yao, Coupled Spin and Valley Physics in Monolayers of MoS_2 and Other Group-VI Dichalcogenides, Phys. Rev. Lett. **108**, 196802 (2012).

[8] K. F. Mak, K. He, J. Shan, and T. F. Heinz, Control of valley polarization in monolayer MoS_2 by optical helicity, Nat. Nanotechnol. **7**, 494 (2012).

[9] H. J. Conley, B. Wang, J. I. Ziegler, R. F. Haglund, S. T. Pantelides, and K. I. Bolotin, Bandgap engineering of strained monolayer and bilayer MoS_2, Nano Lett. **13**, 3626 (2013).

[10] Y. You, X.-X. Zhang, T. C. Berkelbach, M. S. Hybertsen, D. R. Reichman, and T. F. Heinz, Observation of biexcitons in monolayer WSe_2, Nat. Phys. **11**, 477 (2015).

[11] K. F. Mak, K. He, C. Lee, G. H. Lee, J. Hone, T. F. Heinz, and J. Shan, Tightly bound trions in monolayer MoS_2, Nat. Mater. **12**, 207 (2012).

[12] M. Sidler, P. Back, O. Cotlet, A. Srivastava, T. Fink, M. Kroner, E. Demler, and A. Imamoglu, Fermi polaron-polaritons in charge-tunable atomically thin semiconductors, Nat. Phys. **13**, 255 (2016).

[13] D. Van Tuan, B. Scharf, Z. Wang, J. Shan, K. F. Mak, I. Žutić, and H. Dery, Probing many-body interactions in monolayer transition-metal dichalcogenides, Phys. Rev. B **99**, 085301 (2019).

[14] A. Steinhoff, T. O. Wehling, and M. Rösner, Frequency-dependent substrate screening of excitons in atomically thin transition metal dichalcogenide semiconductors, Phys. Rev. B **98**, 045304 (2018).

[15] K. Wang, K. De Greve, L. A. Jauregui, A. Sushko, A. High, Y. Zhou, G. Scuri, T. Taniguchi, K. Watanabe, M. D. Lukin, H. Park, and P. Kim, Electrical control of charged carriers and excitons in atomically thin materials, Nat. Nanotechnol. **13**, 128 (2018).

[16] C. Palacios-Berraquero, D. M. Kara, A. R. P Montblanch, M. Barbone, P. Latawiec, D. Yoon, A. K. Ott, M. Loncar, A. C. Ferrari, and M. Atatüre, Large-scale quantum-emitter arrays in atomically thin semiconductors, Nat. Commun. **8**, 15093 (2017).

[17] R. F. Frindt, Optical absorption of a few unit-cell layers of MoS_2, Phys. Rev. **140**, A536 (1965).

[18] P. Dey, J. Paul, Z. Wang, C. E. Stevens, C. Liu, A. H. Romero, J. Shan, D. J. Hilton, and D. Karaiskaj, Optical Coherence in Atomic-Monolayer Transition-Metal Dichalcogenides Limited by Electron-Phonon Interactions, Phys. Rev. Lett. **116**, 127402 (2016).

[19] T. Jakubczyk, V. Delmonte, M. Koperski, K. Nogajewski, C. Faugeras, W. Langbein, M. Potemski, and J. Kasprzak, Radiatively limited dephasing and exciton dynamics in MoSe2 monolayers revealed with four-wave mixing microscopy, Nano Lett. **16**, 5333 (2016).

[20] K. Hao, L. Xu, P. Nagler, A. Singh, K. Tran, C. K. Dass, C. Schüller, T. Korn, X. Li, and G. Moody, Coherent and incoherent coupling dynamics between neutral and charged excitons in monolayer MoSe2, Nano Lett. **16**, 5109 (2016).

[21] F. Cadiz, E. Courtade, C. Robert, G. Wang, Y. Shen, H. Cai, T. Taniguchi, K. Watanabe, H. Carrere, D. Lagarde, M. Manca, T. Amand, P. Renucci, S. Tongay, X. Marie, and B. Urbaszek, Excitonic linewidth approaching the homogeneous limit in MoS_2-based van der Waals heterostructures, Phys. Rev. X **7**, 021026 (2017).

[22] G. Scuri, Y. Zhou, A. A. High, D. S. Wild, C. Shu, K. De Greve, L. A. Jauregui, T. Taniguchi, K. Watanabe, P. Kim, M. D. Lukin, and H. Park, Large Excitonic Reflectivity of Monolayer $MoSe_2$ Encapsulated in Hexagonal Boron Nitride, Phys. Rev. Lett. **120**, 037402 (2018).

[23] P. Back, S. Zeytinoglu, A. Ijaz, M. Kroner, and A. Imamoğlu, Realization of an Electrically Tunable Narrow-Bandwidth Atomically Thin Mirror Using Monolayer $MoSe_2$, Phys. Rev. Lett. **120**, 037401 (2018).

[24] L. Mennel, M. M. Furchi, S. Wachter, M. Paur, D. K. Polyushkin, and T. Mueller, Optical imaging of strain in two-dimensional crystals, Nat. Commun. **9**, 516 (2018).

[25] J. Hong, Z. Hu, M. Probert, K. Li, D. Lv, X. Yang, L. Gu, N. Mao, Q. Feng, L. Xie, J. Zhang, D. Wu, Z. Zhang, C. Jin, W. Ji, X. Zhang, J. Yuan, and Z. Zhang, Exploring atomic defects in molybdenum disulphide monolayers, Nat. Commun. **6**, 6293 (2015).

[26] H. Wang, C. Zhang, and F. Rana, Ultrafast dynamics of defect-assisted electron-hole recombination in monolayer MoS_2, Nano Lett. **15**, 339 (2015).

[27] J. Xue, J. Sanchez-Yamagishi, D. Bulmash, P. Jacquod, A. Deshpande, K. Watanabe, T. Taniguchi, P. Jarillo-Herrero, and B. J. LeRoy, Scanning tunnelling microscopy and spectroscopy

of ultra-flat graphene on hexagonal boron nitride, Nat. Mater. **10**, 282 (2011).
[28] E. M. Purcell, H. C. Torrey, and R. V. Pound, Resonance absorption by nuclear magnetic moments in a solid, Phys. Rev. **69**, 37 (1946).
[29] D. J. Heinzen, J. J. Childs, J. E. Thomas, and M. S. Feld, Enhanced and Inhibited Visible Spontaneous Emission by Atoms in a Confocal Resonator, Phys. Rev. Lett. **58**, 1320 (1987).
[30] A. M. Vredenberg, N. E. J. Hunt, E. F. Schubert, D. C. Jacobson, J. M. Poate, and G. J. Zydzik, Controlled Atomic Spontaneous Emission from Er^{3+} in a Transparent Si/SiO_2 Microcavity, Phys. Rev. Lett. **71**, 517 (1993).
[31] K. H. Drexhage, H. Kuhn, and F. P. Schäfer, Variation of the fluorescence decay time of a molecule in front of a mirror, Ber. Bunsengesellsch. Phys. Chem. **72**, 329 (1968).
[32] K. H. Drexhage, Influence of a dielectric interface on fluorescence decay time, J. Lumin. **1–2**, 693 (1970).
[33] J. Eschner, C. Raab, F. Schmidt-Kaler, and R. Blatt, Light interference from single atoms and their mirror images, Nature (London) **413**, 495 (2001).
[34] M. A. Wilson, P. Bushev, J. Eschner, F. Schmidt-Kaler, C. Becher, R. Blatt, and U. Dorner, Vacuum-Field Level Shifts in a Single Trapped Ion Mediated by a Single Distant Mirror, Phys. Rev. Lett. **91**, 213602 (2003).
[35] S. Stobbe, J. Johansen, P. T. Kristensen, J. M. Hvam, and P. Lodahl, Frequency dependence of the radiative decay rate of excitons in self-assembled quantum dots: Experiment and theory, Phys. Rev. B **80**, 155307 (2009).
[36] M. L. Andersen, S. Stobbe, A. S. Sørensen, and P. Lodahl, Strongly modified plasmon-matter interaction with mesoscopic quantum emitters, Nat. Phys. **7**, 215 (2011).
[37] P. Tighineanu, M. L. Andersen, A. S. Sørensen, S. Stobbe, and P. Lodahl, Probing Electric and Magnetic Vacuum Fluctuations with Quantum Dots, Phys. Rev. Lett. **113**, 043601 (2014).
[38] R. Brechbühler, F. T. Rabouw, P. Rohner, B. le Feber, D. Poulikakos, and D. J. Norris, Two-Dimensional Drexhage Experiment for Electric- and Magnetic-Dipole Sources on Plasmonic Interfaces, Phys. Rev. Lett. **121**, 113601 (2018).
[39] L. Langguth, R. Fleury, A. Alù, and A. F. Koenderink, Drexhage's Experiment for Sound, Phys. Rev. Lett. **116**, 224301 (2016).
[40] H. Wang, C. Zhang, W. Chan, C. Manolatou, S. Tiwari, and F. Rana, Radiative lifetimes of excitons and trions in monolayers of the metal dichalcogenide MoS_2, Phys. Rev. B **93**, 045407 (2016).
[41] D. B. S. Soh, C. Rogers, D. J. Gray, E. Chatterjee, and H. Mabuchi, Optical nonlinearities of excitons in monolayer MoS_2, Phys. Rev. B **97**, 165111 (2018).
[42] M. Sugawara, Theory of spontaneous-emission lifetime of wannier excitons in mesoscopic semiconductor quantum disks, Phys. Rev. B **51**, 10743 (1995).
[43] T. Byrnes, N. Y. Kim, and Y. Yamamoto, Exciton-polariton condensates, Nat. Phys. **10**, 803 (2014).
[44] D. S. Wild, E. Shahmoon, S. F. Yelin, and M. D. Lukin, Quantum Nonlinear Optics in Atomically Thin Materials, Phys. Rev. Lett. **121**, 123606 (2018).
[45] S. Zeytinoğlu, C. Roth, S. Huber, and A. İmamoğlu, Atomically thin semiconductors as nonlinear mirrors, Phys. Rev. A **96**, 031801(R) (2017).
[46] Y. Yu, C. Li, Y. Liu, L. Su, Y. Zhang, and L. Cao, Controlled scalable synthesis of uniform, high-quality monolayer and few-layer MoS_2 films, Sci. Rep. **3**, 1866 (2013).
[47] Y.-H Lee, X.-Q. Zhang, W. Zhang, M.-T. Chang, C.-T. Lin, K.-D. Chang, Y.-C. Yu, J. T.-W. Wang, C.-S. Chang, L.-J. Li, and T.-W. Lin, Synthesis of large-area MoS_2 atomic layers with chemical vapor deposition, Adv. Mater. **24**, 2320 (2012).
[48] C. Rogers, D. Gray, N. Bogdanowicz, and H. Mabuchi, Laser annealing for radiatively broadened $MoSe_2$ grown by chemical vapor deposition, Phys. Rev. Mat. **2**, 094003 (2018).
[49] P. J. Zomer, M. H. D. Guimarães, J. C. Brant, N. Tombros, and B. J. van Wees, Fast pick up technique for high quality heterostructures of bilayer graphene and hexagonal boron nitride, Appl. Phys. Lett. **105**, 013101 (2014).
[50] F. Pizzocchero, L. Gammelgaard, B. S. Jessen, J. M. Caridad, L. Wang, J. Hone, P. Bøggild, and T. J. Booth, The hot pick-up technique for batch assembly of van der Waals heterostructures, Nat. Commun. **7**, 11894 (2016).
[51] N. Bogdanowicz, C. Rogers, D. Gray, C. Timossi, F. Marazzi, J. Wheeler, and I. Galinskiy, mabuchilab/Instrumental: 0.5, version 0.5 (2018), http://doi.org/10.5281/zenodo.2556399
[52] See Supplemental Material at http://link.aps.org/supplemental/10.1103/PhysRevResearch.2.012029 for additional experimental methods and details of the reflectance model and fitting procedures.
[53] D. Meschede, W. Jhe, and E. A. Hinds, Radiative properties of atoms near a conducting plane: An old problem in a new light, Phys. Rev. A **41**, 1587 (1990).
[54] Y. Liu, J. Lin, G. Huang, Y. Guo, and C. Duan, Simple empirical analytical approximation to the Voigt profile, J. Opt. Soc. Am. B **18**, 666 (2001).
[55] J. J. Olivero and R. L. Longbothum, Empirical fits to the Voigt line width: A brief review, J. Quant. Spectrosc. Radiat. Transfer **17**, 233 (1977).
[56] F. Wooten, *Optical Properties of Solids* (Academic Press, San Diego, 1972), Chap. 3.
[57] C. C. Katsidis and D. I. Siapkas, General transfer-matrix method for optical multilayer systems with coherent, partially coherent, and incoherent interference, Appl. Opt. **41**, 3978 (2002).
[58] Y. Zhou, G. Scuri, J. Sung, R. J. Gelly, D. S. Wild, K. De Greve, A. Y. Joe, T. Taniguchi, K. Watanabe, P. Kim, M. D. Lukin, and H. Park, Controlling excitons in an atomically thin membrane with a mirror, Phys. Rev. Lett. **124**, 027401 (2020).
[59] H. H. Fang, B. Han, C. Robert, M. A. Semina, D. Lagarde, E. Courtade, T. Taniguchi, K. Watanabe, T. Amand, B. Urbaszek, M. M. Glazov, and X. Marie, Control of the Exciton Radiative Lifetime in Van Der Waals Heterostructures, Phys. Rev. Lett. **123**, 067401 (2019).
[60] J. Horng, Y.-H. Chou, T.-C. Chang, C.-Y. Hsu, T.-C. Lu, and H. Deng, Engineering radiative coupling of excitons in 2d semiconductors, Optica **6**, 1443 (2019).